Preparation of solvent resistant supports through formation of a semi-interpenetrating polysulfone/polyacrylate network using UV cross-linking, part 1 : selection of optimal UV curing conditions

Preparation of solvent resistant supports through formation of a semi-interpenetrating polysulfone/polyacrylate network using UV cross-linking - Part 2: Optimization of synthesis parameters for UV-LED curing

Peter-Renaat Van den Mooter[a,1], Nick Daems[b,c,1], Ivo F. J. Vankelecom[a,*]

[a] Membrane Technology Group – cMACS – Faculty of Bioscience Engineering, KU Leuven, Celestijnenlaan 200F, Box 2454, 3000 Heverlee, Belgium

[b] Applied Electrochemistry and Catalysis, U Antwerpen, Campus Drie Eiken, Universiteitsplein 1, 2610 Wilrijk, Belgium

[c] Separation & Conversion Technologies, Flemish Institute for Technological Research (VITO), 2400 Mol, Belgium

[*] Corresponding author. E-mail address: ivo.vankelecom@kuleuven.be (I.F.J. Vankelecom); Tel.: +3216321594

[1] Equal contribution

Abstract

Concerns of energy shortage and pollution, have rapidly increased the demand for efficient separation processes. In this respect, solvent resistant nanofiltration has become an emerging technology with great potential as an energy-efficient and waste-free separation method. Unfortunately, the lack of sufficient stability (especially chemical stability of the support) still restricts the utilization of this separation technique to the more mild industries, leaving several unexploited. As already detailed in part I of this research, one promising approach to increase the chemical stability of supports, used afterwards as starting point for the synthesis of thin film composite nanofiltration membranes, is cross-linking polymeric UF membranes by UV-irradiation. Whereas in the previous part, the 365 nm UV-LED light was selected as the best setup to achieve a high cross-linking efficiency at high throughputs, in this second part the impact of (non-)compositional parameters on the cross-linking efficiency was investigated. The most important parameters with the largest impact on the degree of conversion (DC) were shown to be the cross-linker content, the membrane thickness and the incorporation of a non-woven support. Finally and more importantly, after curing the membranes did not only show enhanced solvent stabilities (viz. part I), they also exhibited greater physical strength while at the same time maintaining the retention at a similar level as the non-cured membrane clearly indicating their industrial importance.

Keywords: Photo-irradiation; UV cross-linking; UV-LED; Solvent Resistant Support; Upscaling

No conflicts of interest.

1. Introduction

Concerns of energy shortage and pollution, have rapidly increased the demand for efficient separation processes [1,2]. In the chemical and pharmaceutical industry, 40-70 % of the capital and operation costs are still attributed to separation processes, such as the widely used distillation, crystallization, extraction and adsorption [3,4]. This indicates the importance of choosing the most efficient separation technology for every application, not only from a performance point of view, but also with respect to energy costs. In this search, membrane technology emerges as an attractive option, because it can be operated continuously and has several attractive properties, like a low energy demand, ease of operation and mild operating conditions. Moreover, membrane properties can be easily modified to fit specific separation purposes and membrane technology can be readily combined with other processes [2,5,6].

Nanofiltration (NF) is a pressure-driven (5-20 bar) membrane process, which is gaining a lot of attention because of its broad application potential. Originally, large-scale applications of these membranes mainly included aqueous applications, using hydrophilic polymers [6]. Recently, NF-membranes have also been used in solvent-based applications, requiring high chemical stability of the membrane. Solvent resistant nanofiltration (SRNF), also known as organic solvent nanofiltration (OSN), has thus become an emerging technology with great potential as an energy-efficient and waste-free separation method e.g. in food and pharmaceutical industries, or in petrochemical applications [7–12]. Many membrane materials used for NF applications however, fail under extreme conditions, such as extreme pH (above 12 or below 2) or in harsh solvents that easily dissolve most polymers used for NF applications (i.e. aprotic polar solvents, such as dimethylformamide (DMF), *N*-methylpyrrolidinone (NMP), dimethylsulfoxide (DMSO), etc.) [12–15]. Examples of industrial applications that require such extreme pH conditions, include the treatment of pulp, paper or mining effluents, and the separation of hemicellulose from concentrated alkaline processes [16–20].

An interesting strategy to obtain SRNF membranes, which are stable in extreme conditions, is to synthesize thin film composite (TFC) membranes starting from chemically stable asymmetric ultrafiltration (UF) supports. A more selective top-layer is then deposited on these supports. During the final application, both layers have to be resistant. Also during the deposition of the top-layer, the support is supposed to remain stable. As for the support, currently polyacrylonitrile (PAN) [21], polyimide (PI) [9,22] and polysulfone (PSU) [9,13,23,24] are most often used. The latter, PSU membranes, for example, have strong thermal and mechanical properties which make it an ideal support candidate for a broad range of membrane applications [23,25–28]. However, their low resistance to e.g. N-methylpyrrolidone (NMP), tetrahydrofuran (THF) or ethyl acetate, makes them

still of limited use as support for SRNF [24,29,30]. These polymeric membranes generally possess an asymmetric cross-sectional morphology and are called integrally skinned asymmetric membranes (ISA). ISA membranes consist of a less porous top-layer (0.1 to 1 µm thickness) supported by a much thicker, porous sublayer (50 to 150 µm thickness). These membranes are prepared by non-solvent induced phase separation (NIPS) where a polymer solution is cast on a support, followed by immersion in a non-solvent bath where demixing and polymer precipitation occurs [3,5]. To further increase solvent stability, these membranes have to be modified through cross-linking. Cross-linking the polymer chains can be achieved by means of e.g. a thermal treatment [31–33], chemical reactions [29,34–37] or photo-irradiation using IR- [38,39], UV-sources [24,40–43] or electron beam (EB) [41,44], of which the latter is interesting because of some unique features, i.e. spatial resolution, precise control of the process, limited use of chemicals, mild conditions, selectivity of chemical reactions, etc. [45].

This study is the second part of our research that deals with the preparation of a semi-interpenetrating polysulfone/polyacrylate network using UV cross-linking [46]. The complete study can be seen as a feasibility study towards upscaling a semi-interpenetrating polymer network (SIPN) preparation by UV cross-linking in order to obtain a more chemically stable UF membrane, which can then be used in a next step to obtain solvent-stable SRNF membranes. In the first part, the optimal UV-curing unit was selected using a standard PSU membrane composition and a proof of the chemical stability after cross-linking was obtained [43,47–49]. UV-LED curing was thus shown to be an easy and versatile method to synthesize cross-linked UF supports. In this second part, the impact on the cross-linking degree of various (non-)compositional parameters, which are essential towards upscaling, will be investigated. As a UV-LED system was most promising [46], only this setup will be further investigated. A critical aspect in the parametric screening of the cross-linking degree lays in the choice of a suitable type and concentration of photo-initiator and cross-linker. The photo-initiator has to be chosen such that it can (1) produce radicals in the available light spectrum, and (2) ensure penetration of the UV-light throughout the whole thickness of the solidified membrane. The latter is quite challenging as membranes are generally opaque and relatively thick. Additionally, the choice of the cross-linker also influences the UV-curing efficiency, as their functional groups and water solubility (of importance during the phase inversion process to prevent leaching) can have a major impact on the resulting cross-linking degree [24].

The aim of this study is thus the practical screening of parameters during NIPS/UV membrane synthesis using a UV-LED curing system (i.e. type and concentration of photo-initiator and cross-linker, cast film thickness and choice of support material during UV-radiation), to obtain supports

which are stable in a wide range of solvents. After screening and tuning of these parameters, the composition with high degree of conversion (DC) for a short radiation time was selected. These supports, with a chemical composition as previously described [46] (i.e. acyl phosphine oxide-based photo-initiator in combination with a pentaacrylate crosslinker), will subsequently be upscaled to industrial dimensions and used in preparation of more selective SRNF membranes (e.g. TFC membranes via interfacial polymerization) [9,13].

2. Experimental

2.1. Materials

Commercially available PSU (Udel® P-1700 LCD, $M_n \sim 21{,}000$ g mol^{-1}) was kindly supplied by Solvay and dried at 100 °C for 24 h prior to use. N,N-dimethylformamdide (DMF, 99.8 % VWR BDH Prolabo), tetrahydrofuran (THF, anhydrous, containing 250 ppm BHT as inhibitor, ≥ 99.9 %, Sigma-Aldrich) and Rose Bengal (RB, MW 1017 Da, Sigma Aldrich) were used as received. Acrylate monomer dipentaerythritol penta-acrylate (SR399LV, Sigma Aldrich) (Table 1), was used as cross-linker. The acyl phosphines, 2,4,6-trimethylbenzoyl-diphenylphosphineoxide (TPO, Sigma-Aldrich) and bis(2,4,6-trimethylbenzoyl)-phenylphospineoxide (IR819, TCI Europe NV) (Table 1), were applied as photo-initiators.

Table 1. Photo-initiators and cross-linker used in this study.

Compound	Name	Structure
TPO	2,4,6-trimethylbenzoyl-diphenylphosphineoxide (Darocur™ TPO)	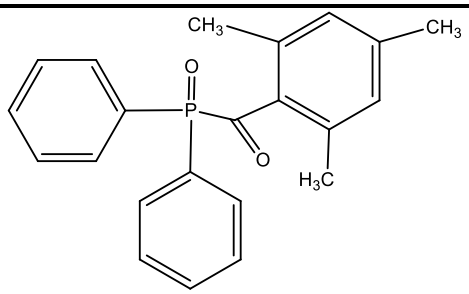
IR819	bis(2,4,6-trimethylbenzoyl)-phenylphospineoxide (Irgacure™ 819)	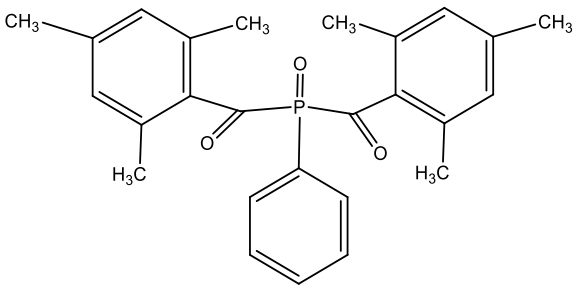

SR399LV	Dipentaerythritol penta-acrylate (Sartomer™ SR399 LV)	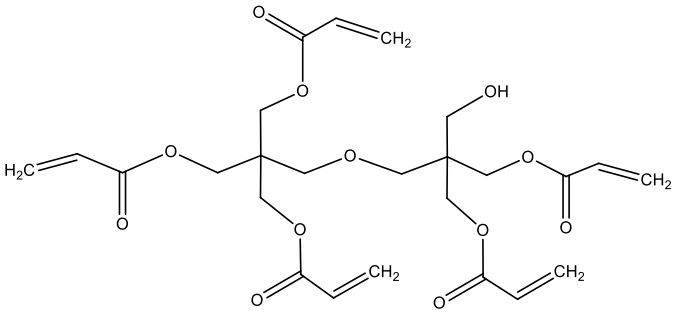

2.2. Membrane preparation and UV cross-linking

An asymmetric, polymeric membrane was synthesized from PSU via NIPS (Figure 1) [7]. A viscous 21.0 wt% PSU solution in DMF was stirred at 80 °C for 3 h. After cooling, 2.5 wt% of cross-linker, 3.0 wt% of a photo-initiator (PhIn) and THF, as volatile co-solvent, were added unless stated otherwise. The DMF/THF ratio was set to 85/15. The solution was then covered by aluminum foil and stirred until a homogeneous mixture was obtained. Subsequently, the mixture was left overnight for degassing. Next, membranes with a wet film thickness of 200 µm were cast on a glass plate at a speed of 1.29 m/min using an automated casting knife (Braive Instruments, Belgium). Prior to immersion in the coagulation (i.e. deionized water) bath, the cast film was exposed to air for 30 s in order to evaporate THF and create a thin, denser top layer. Afterwards, the resulting membrane was stored in the dark in deionized water until UV-curing. All steps were performed in the dark at of 20 ± 2 °C under ambient atmosphere with a relative humidity (RH) of 30 ± 10 %. The temperature of coagulation bath was 18 °C. The membrane was then cut into strips of 15 x 45 mm samples and dipped dry with tissue paper before passing them through a UV-LED unit by fixing them on a black non-porous metallic substrate.

UV cross-linking was performed under ambient atmosphere using UV-LED irradiation of 365 nm. After UV-curing, the samples were kept in aluminum foil until physicochemical characterization. The method described here is referred to as the NIPS/UV method.

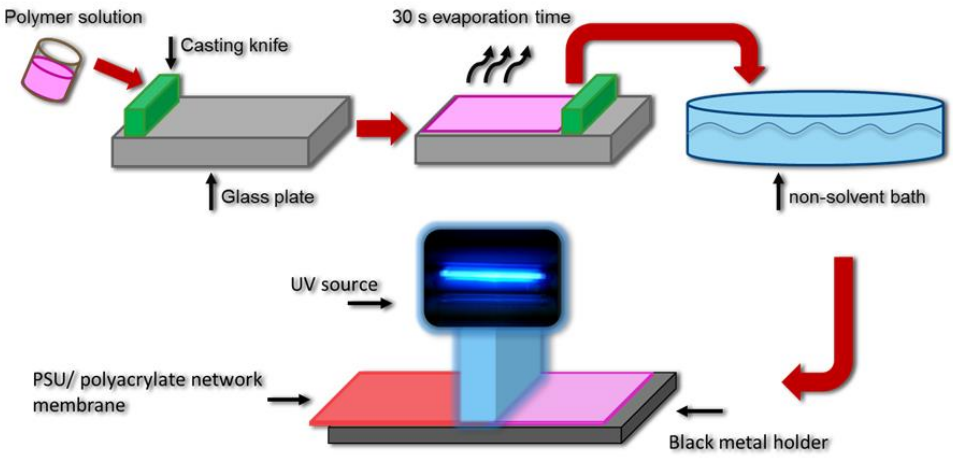

Figure 1. Non-solvent induced phase separation (NIPS), followed by UV-LED curing.

After selection of the most optimal chemical composition, a new membrane coupon was used for each subsequent experiment where the other parameters (e.g. coupon dimension, photo-initiator type, film thickness, etc.) were changed.

UV-light emitting diode (LED)

Two UV-LED systems, i.e. OmniCure® - AC8300 (Polytec GmbH, DE) and Semray® - UV4003 (UVio Ltd., UK), were used for UV-curing. Both lamps have a specific wavelength of 365 nm, a typical peak irradiance of 2.0 W/cm² at a distance of 35.0 mm from the substrate and at an exit angle of 60°. As both systems have comparable specifications, they will result in comparable curing efficiencies. The reader is referred to the online available literature for additional technical data concerning the lamps [50,51]. The parameters controlled here were peak power, frequency and duration. It is important to note here that for every parameter setting, a fresh, untreated membrane sample was taken. Firstly, the UV-LED system from Polytec was used to screen compositional parameters and to optimize the chemical composition towards maximum degree of conversion (DC). Secondly, the UV-LED system from Semray was used to screen non-compositional parameters and finally for comparison with the UV-LED system of Polytec.

2.3. Filtration experiments

A high-throughput filtration setup containing 8 membrane positions, with an active filtration area of 0.2×10^{-3} m² operated at 5 to 15 bar, was used to evaluate the membrane performance. This set-up has the capacity to simultaneously screen membrane coupons (min. 2 of each membrane type) in a dead-end mode. An aqueous solution of 17.0 µM RB was used as feed and stirred at 360 rpm to minimize concentration polarization. First permeate samples were discarded to allow for the membranes to reach

a steady state before starting the collection of permeate samples (at least 2 ml) for actual analysis. The permeance (P) was determined by the following equation (1);

$$P = \frac{V}{A \,.\, t \,.\, \Delta P} \quad (1)$$

with V as permeate volume (L), A as active membrane area (i.e. 0.2 x 10^{-3} m^2), t as permeate collection time (h) and ΔP as pressure (bar). The retention (R) was determined by equation (2);

$$R = \left(1 - \frac{C_p}{C_f}\right) . 100\ \% \quad (2)$$

with C_p and C_f as permeate and feed solute concentration, respectively. The dye concentrations in feed and permeate were analyzed using a Shimadzu UV – 1800 UV/VIS spectrophotometer at room temperature.

2.4. Membrane characterization

2.4.1. ATR-FTIR

The cross-linking efficiency was determined by following the conversion of the acrylate double bonds to single bonds by an Attenuated Total Reflectance – Fourier Transform Infrared Spectroscopy (ATR-FTIR) spectrometer (VARIAN 620 IR FT-IR Imaging Microscope). The spectrometer is equipped with a Germanium Slide PN 066-4903 ATR crystal with a resolution of 4 cm^{-1} [52]. The top of each membrane sample was scanned on 2 or 3 spots for 64 times between 4000 and 400 cm^{-1}. The conversion efficiency was then calculated by the ratio between UV-cured and non-cured membranes, which were kept in aluminum foil until measurement, according to the following equation:

$$Degree\ of\ conversion = \left(1 - \frac{\left(\frac{C=C}{C=O}\right)_{cured}}{\left(\frac{C=C}{C=O}\right)_{non-cured}}\right) . 100 \quad (3)$$

with absorbance peaks for the C=C group between 800 and 820 cm^{-1} and for the C=O group between 1715 and 1735 cm^{-1} [53]. The C=O group absorbance does not alter during curing and thus serves as a reference. It is believed that polymer degradation might take place simultaneously with the cross-linking process. However, when comparing the ATR-FTIR spectra of a membrane coupon treated with only one pulse to that of a coupon that underwent 10 pulses and showed clear signs of degradation (i.e. visually observed color changes [46]), no significant differences can be observed. Especially, no new peaks seem to arise that could be attributed to degradation.

Due to the 5 reactive groups of the cross-linker, a DC of 40% or more was considered to be a minimal requirement for successful reaction. Theoretically, a minimal DC of 40% would imply that a reaction

occurred between at least 2 of the 5 reaction groups of the cross-linker with 2 other acrylate groups. This would at least result in a polymer network system.

Each composition or type of membrane was radiated as function of time with a 365 nm UV-LED lamp, i.e. going from 10 to 400 s. The range of radiation times was determined by a combination of passage speed through the anticipated pilot-scale system (0.1-3.0 m/min) [54] and the available emission window of the UV unit (300 mm x 45 mm). The DC for each type of membrane or chemical composition, are the highest DC that could be achieved by altering the radiation time within the available time frame (0 to 400 s).

2.4.2. ATR-FTIR Measurement spots for large samples

Figure 2 shows schematically the top view of a large membrane coupon. ATR-FTIR measurements were taken according to spots indicated in the Figure.

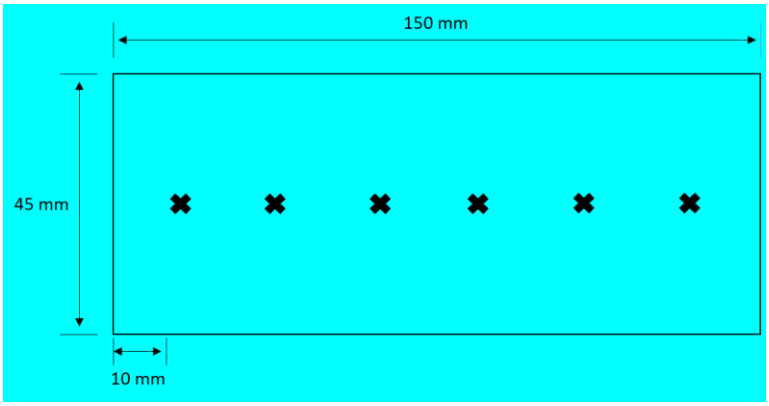

Figure 2. Schematic of the large membrane coupon and the locations of each point of measurement.

2.4.3. UV/VIS spectrophotometer

To verify the wavelength of maximal absorption of the different PhIns, their UV/VIS spectra (range 190 – 1100 nm) were measured utilizing 3.0 wt% solutions of PhIn in DMF on an Agilent 8453 UV/VIS spectrophotometer at room temperature. A quartz cell with a path length of 10 mm was used.

2.4.4. Tensile strength measurements

Immediately after UV-curing, the membrane coupons were cut in pieces with a width of 10 mm and a length of 50 mm. Next, they were wrapped in aluminium foil and stored in a light-proof container until the measurements. The tensile strength measurements were performed at room temperature on an Instron 5943 (USA) tensile machine with a 1 kN load cell. The membrane coupon was fixed by two vertical clamps and calibrated for length and load before stretching. The two clamped ends were pulled

apart at a rate of 1.0 mm/ min. The load (N) and tensile extension at load (mm) were measured as function of time (s) for a constant tensile strain of 5 mm. From these measurements, the maximum load and the tensile extension at maximum load were determined at the rupture point of the sample.

3. Results and discussion

3.1. Screening of compositional parameters

The acrylate conversion under UV-radiation has to be as high as possible to improve membrane stability and thus applicability. During screening of the radiant range from 0 to 400 s, the concentration of PSU was kept constant at 21.0wt% while the ratio between cross-linker and photo-initiator was varied, as shown in Table 2. The concentrations of cross-linker SR399LV and photo-initiator TPO were varied between 2.5-10.0 wt% and 3.0-12.0 wt%, respectively. Even higher concentrations of both resulted in incomplete dissolution, thus making it impossible to cast defect-free membranes. For every compositional parameter, two variables were analyzed and will be discussed in this research: (1) the change of conversion with radiation time and (2) the maximum conversion that could be achieved. The hypotheses tested were that higher DC values are obtained at increased cross-linker concentrations, and that an optimum exists for the PhIn in free radical polymerizations.

Impact of cross-linker content

The DC as a function of the radiation time was first studied for a constant photo-initiator concentration of 3.0 wt% and a variable acrylate monomer concentration (M1-M4). The UV absorption spectrum of acrylate monomer SR399 (in ethanol) showed no significant UV absorption at 365 nm, as given in Figure 3. Therefore, it was considered that no polymerization could start upon UV radiation nor could the monomer largely influence the UV light penetration depth by absorption [55].

As the acrylate concentration increases, longer radiation times are required to reach that first maximum (Figure 4), as there are simply more functional groups to react. Longer radiation times than those indicated on Figure 4 resulted in a changed visual appearance of the samples (i.e. turning brown and later on even black; in addition, some kind of melting appeared). Possibly, these colour changes can be linked to occurrence of side reactions, e.g. disproportion reactions, as mentioned in *Hancock et. al.* [55]. Whether they are a direct consequence of the irradiation or rather an indirect consequence through the increased temperature of the samples, remains unclear. Indeed, the temperature, as measured at 1 cm above e.g. the M4 sample, was found to be 32 °C after 25 s of irradiation and 134 °C after 200 s. The black stainless steel substrate to which the membrane samples were fixed, thus clearly converted the radiation into heat.

Membrane M4 clearly showed the highest DC over the complete radiation time range. No statistical difference in conversion could be observed for M1-3. As radiation time increased, a certain decrease

in DC was surprisingly observed. Possibly, this could be due to thermally induced side reactions, taking into account the very high temperatures realized in the samples.

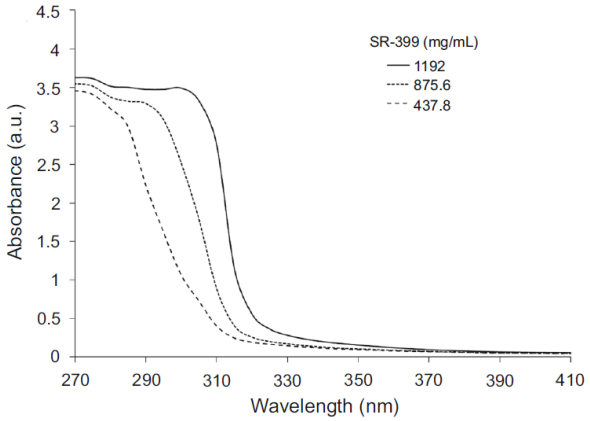

Figure 3. UV absorption spectra of SR399 dispersed in ethanol for 3 different weight percent values of C=C concentrations: 100 % (1,192 mg ml^{-1}), 80 % (875.6 mg ml^{-1}) and 40 % (437.8 mg ml^{-1}). Adapted from [57].

A maximum DC of 70.0 ± 2.1 % was observed for a cross-linker concentration of 10.0 wt% (Table 2). As the concentration of cross-linker increases for a constant photo-initiator content, the probability increases for photo-initiator radicals to react with cross-linker monomer and thus potentially polymerize, explaining the higher conversion [45]. This can be observed from the increasing conversion of M1 to M4 and supports the stated hypothesis.

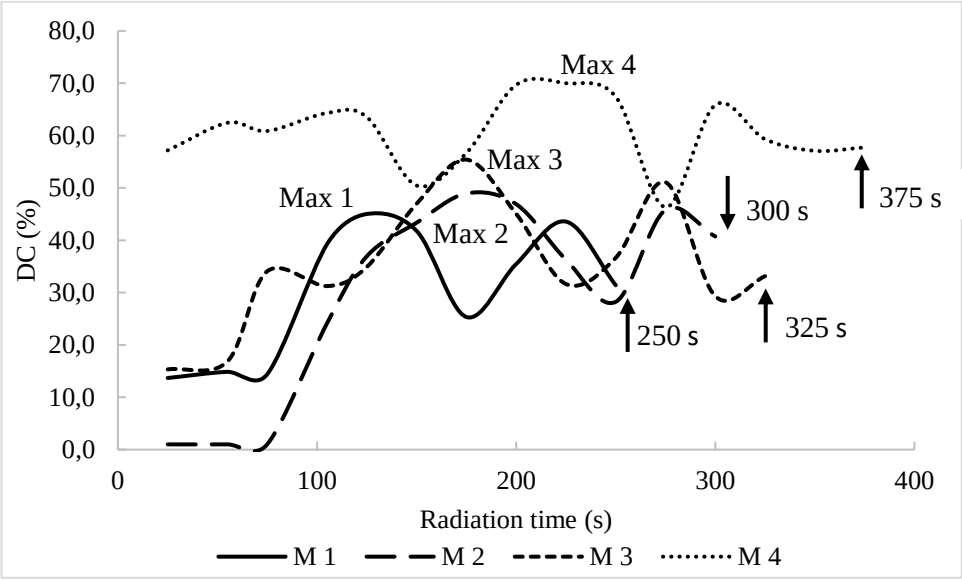

Figure 4. DC for increasing cross-linker concentration (%) as a function of UV radiation time (s). UV-radiation was performed with UV-LED from Polytec.

Table 2. DC as a function of membrane compositions for different photo-initiator and cross-linker ratio. UV-radiation was performed with UV-LED from Polytec.

Membrane no.	Cross-linker (wt %)	Photo-initiator (wt %)	Maximum DC (%)	Radiation time of maximum DC (s)
M1	2.5	3.0	45.0 ± 4.1	125
M2	5.0	3.0	48.9 ± 2.6	175
M3	7.5	3.0	55.4 ± 3.9	175
M4	10	3.0	70.0 ± 2.1	225
M1	2.5	3.0	45.0 ± 4.1	125
M5	2.5	6.0	7.5 ± 2.3	35
M6	2.5	9.0	12.8 ± 2.2	35
M7	2.5	12.0	10.5 ± 1.5	35
M1	2.5	3.0	45.0 ± 4.1	125
M8	5.0	6.0	39.2 ± 4.4	105
M9	7.5	9.0	39.9 ± 3.7	65
M10	10.0	12.0	41.0 ± 3.5	78

Impact of photo-initiator content

Next, the radiation time range for a constant cross-linker concentration of 2.5 wt% and a variable photo-initiator concentration was studied (Figure 5). A significant decrease in radiation time was observed when increasing the photo-initiator concentration above 3 wt% since samples M5-M7 visually changed color at radiation times longer than 65, 85 or 105 s, respectively. Therefore, the investigated radiation time range was shortened to 105 s. It was suggested that the efficiency of absorption of the incident radiation by the PhIn increases with the PhIn concentration, resulting in more radicals. A possible explanation, according to [24,45,58–60], is that increasing the PhIn concentration results in a large amount of free radicals, which quickly generate a polymer network. Within this concept of chain-growth polymerization, the kinetic chain length (i.e. average number of monomers reacting with a given radical from its initiation to its termination) was known to be inversely proportional to the radical concentration. Therefore, the average length of the polymers in this network was suggested to decrease with increasing PhIn concentration. Additionally, according to [61,62], an increase in PhIn content at constant cross-linker concentration will result in a decreased probability of spontaneous collision of the PhIn with the cross-linker and an increase in recombination of the radicals. Moreover, some PhIn molecules will go from the triplet state to the ground state due to their short life,

making them quench before being used in polymerization. These reactions influence the photopolymerization and result in a decreased acrylate chain-growth polymerization. These combined effects could explain the weaker physical properties of the membrane and thus lower decomposition temperature (i.e. decreased radiation time) of the obtained polymer network [45,60]. As shown in Figure 3, one clear DC maximum was observed at a same radiation time of 35 s for the M5-M7 membrane compositions. Additionally (Table 2), after the initial decrease in DC (from M1 to M5), the PhIn concentration only has a minor impact on the DC. A maximum DC of only 12.8 ± 2.2 % was obtained for composition M 6 in particular. The lower DC in presence of higher TPO contents, is believed to be caused by the larger number of generated radicals that negatively influences the chain-growth polymerization (as mentioned before). These low molecular weight decomposition products of the PhIn in the membrane could act as plasticizers [24,60].

To conclude, the hypothesis as stated above with respect to the optimum PhIn content could neither be rejected nor accepted as an optimum could still be apparent for lower PhIn concentrations although 3 wt% is generally used in literature [24,58,63].

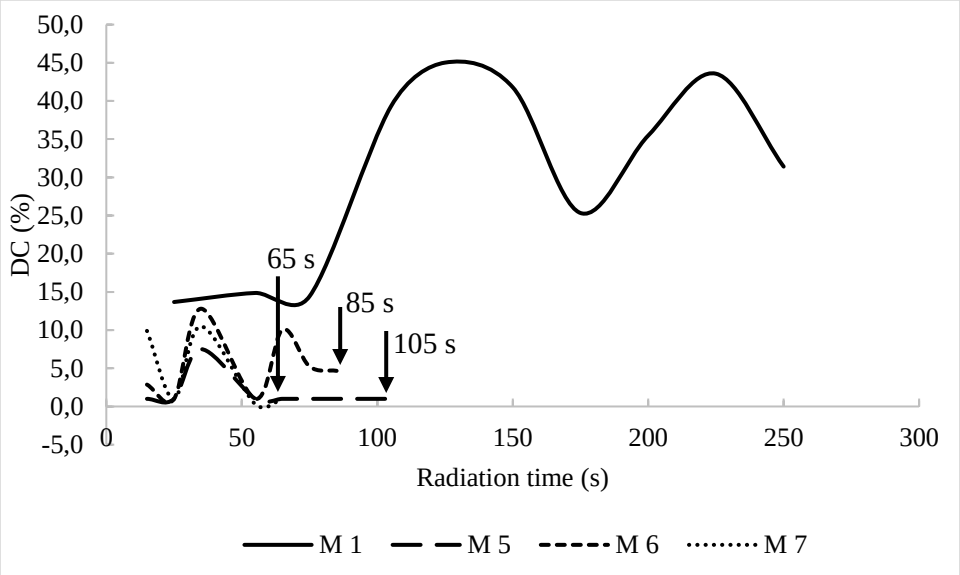

Figure 5. DC for increasing photo-initiator concentration (%) as a function of UV radiation time (s). UV-radiation was performed with UV-LED from Polytec.

Impact of simultaneous increase in cross-linker and photo-initiator content at constant ratio

For Figure 6, both photo-initiator and cross-linker concentrations were varied while their ratio was kept constant. A clear maximum was observed for compositions M 8-M 10, all reaching quasi the same DC as membrane M 1, i.e. 45.0 ± 4.1 %. Additionally, the maximum radiation time was lower compared to those obtained with increasing cross-linker content and higher compared to those achieved with increasing amount of PhIn. This indicates that the impact of changing PhIn

concentration, as described previously, is larger than the effect of the changing cross-linker concentration.

The optimum conversion that could be achieved was also in between the optimal conversion achieved when (1) increasing PhIn concentration and (2) increasing the cross-linker concentration (Table 2). As the ratio was kept constant, increasing the cross-linker and photo-initiator concentrations didn't significantly improve the DC. It was comparable to the DC of the initial composition with a 2.5 wt%/3.0 wt% cross-linker/photo-initiator ratio.

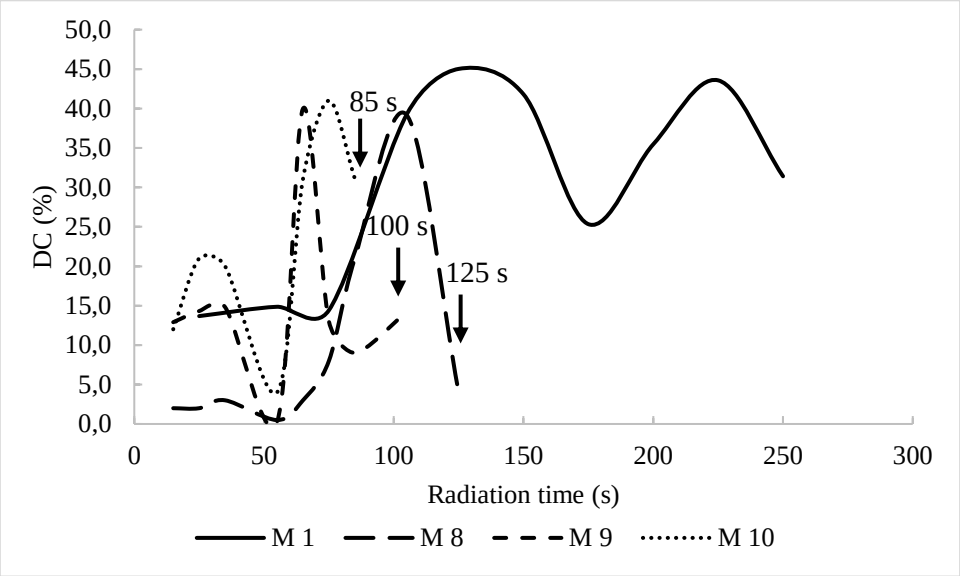

Figure 6. DC for simultaneous increasing of cross-linker and photo-initiator concentration while keeping their ratio constant (%) as a function of UV radiation time (s). UV-radiation was performed with UV-LED from Polytec.

To conclude, a maximal DC of 70.0 ± 2.1 % was thus observed for a cross-linker concentration of 10.0 wt% and a 3.0 wt% of photo-initiator. This chemical composition will be further used in the screening of the non-compositional parameters.

3.2. Reproducibility of the membrane preparation method

The reproducibility was evaluated for the optimal chemical composition M4 over the complete radiant time (i.e. 0 - 400 s). A similar trend in DC could be observed for all 3 replica, as given in Figure 7.

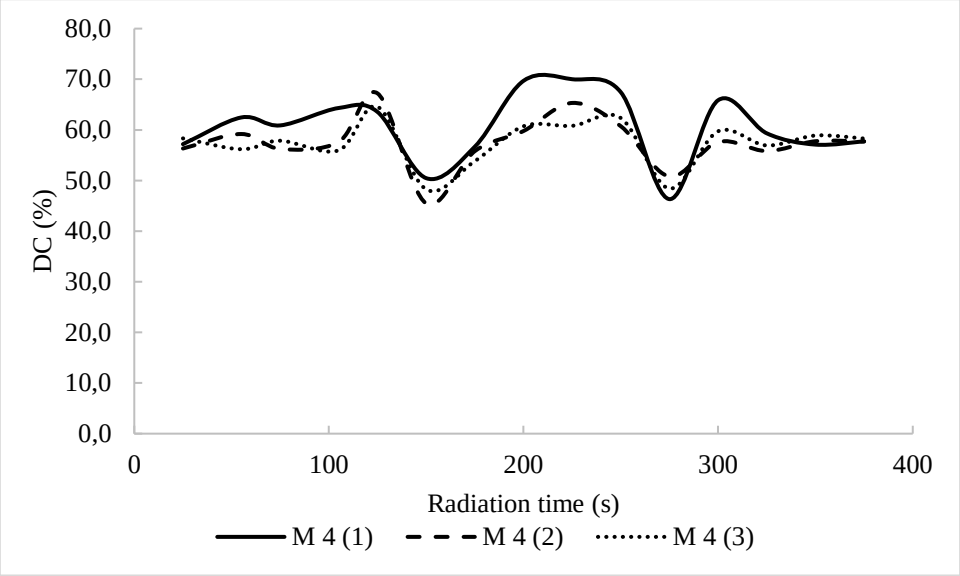

Figure 7. DC as function of radiation time (s) was repeated for 3 times with membrane composition M 4. UV-radiation was performed with UV-LED from Semray.

3.3. Sample size

A freshly prepared M 4 membrane coupon was further used to compare the curing efficiency of samples with a different size of the cured surface area at constant irradiation time (i.e. 125 s). The cured area ranged from 200 mm² (2 cm x 1 cm, small coupon) to 6750 mm² (15 cm x 4.5 cm, large coupon).

Table 3. DC for membrane coupons M 4, for small and large UV - cured area (200 mm² and 6750 mm², respectively). UV-radiation was performed with UV-LED from Semray.

Membrane type	DC (%)	Radiation time (s)
Small coupon	65.1 ± 2.9[1]	125
Large coupon	65.4 ± 0.3	125

[1]Average value obtained from the reproducibility experiments performed in paragraph 3.2.

Based on the obtained results (Table 3) it can be concluded that the UV-curing occurs homogeneously also for larger samples, as indicated by the even smaller standard deviations (6 spots were measured according to location specified in section 2.3). No significant difference was thus observed when the

cured area was increased by a factor of 34, proving the feasibility of upscaling this curing process for the given chemical composition with the UV-LED curing system.

3.4. Type of photo-initiator

The photo-initiator TPO, with an optimal absorbance wavelength of 360 nm (Figure 8), was used in all above experiments. In the next section, another photo-initiator type, IR 819 with a slightly different optimal absorbance wavelength (i.e. 365 nm which is identical to the wavelength of the UV lamp), was used for comparison, utilizing a membrane coupon with optimal conditions as determined in the previous sections (i.e. 3.0 wt%, PhIn, 10.0 wt% cross-linker, curing area of 200 mm² and irradiation time of 250 s).

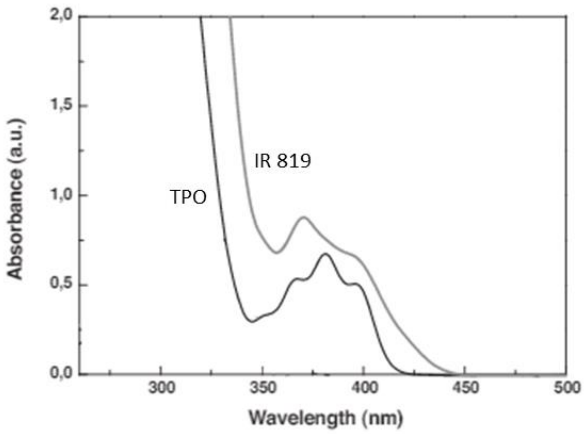

Figure 8. UV-vis spectra of TPO and IR 819. Adapted from [24].

Only a statistically insignificant higher DC was achieved when the initial photo-initiator (TPO) was used: 63.7 ± 3.2 % *vs* 61.9 ± 4.3 . By combining the small difference in optimal absorbance between the two PhIns with the fact that UV-LED systems are known to radiate 5 nm above and below the maximal wavelength, this lack of difference was actually expected [50].

3.5. Continuous compared to pulsed UV-radiation

The UV-LED system has 2 possible radiation modes: pulsed and continuous. For the optimal chemical composition, both modes were evaluated using comparable cumulative radiation times (10 x 10 s *vs* 100 s). The time in between pulses was kept as low as possible (i.e. 5 s) in order to avoid the cooling down of the sample. As such, it is believed that the impact of temperature differences between both modes could be reduced to a minimum and will thus not play a significant role in the observed differences in conversion. Based on these experiments, the continuous radiation mode was selected as best, as it resulted in a somewhat higher, though strictly not statistically relevant, DC (62.3 ± 7.1 % *vs* 51.9 ± 7.3 %). The better result for continuous radiation could be expected as it is known that non-

transparent coatings are challenging for UV-curing. Therefore, it is suggested that a longer UV-irradiation or higher doses of light are required for depth curing [49]. These results thus support the use of the UV-LED system in a continuous manner.

3.6. Screening of non-compositional parameters

As a thinner polymer film requires less consumables and thus results in a better cost balance, different film thicknesses were tested, applying the same optimal conditions as described previously (Table 4). As the thickness decreased, the DC_{max} decreased. UV-cured films are known to follow a surface to depth crosslinking gradient [24,64]. This will imply that a longer UV irradiation, or a higher dose of light, is required for complete depth-curing of thick films, as can be seen in Table 4. The thinner the film becomes, the lower the radiation time needed to obtain DC_{max} (250 s to 125 s for 200 µm and 50 µm, respectively). The penetration of UV-light was thus more efficient for thinner films. On the other hand, as described by Baxter et al., a thicker film led to a considerable increase in the amount of heat retained in the film immediately after irradiation.[62] A temperature increase is known to improve the extent of curing. This could be explained by the decreased viscosity upon heating which leads to increased mobility of the growing polymer chains and of the remaining monomer and PhIn radicals, resulting in a higher probability for collision. This effect was not only observed with an increase in maximum DC but also when the DC for a constant radiation time of 125 s was measured. Gradually lower DC values along increasing film thickness were observed.

All these phenomena, linked to the thickness of the film, thus influence the DC_{max} after curing. A thinner film will result in a more efficient UV-radiation over the complete membrane depth and the maximum DC will be obtained more rapidly. Thicker films need more time for UV depth-curing but result in an increased maximum DC due to more efficient heat retention in the film.

Table 4. DC (%) for different membrane casting thickness (200, 150, 100, 50 µm). UV-radiation was performed with UV-LED from Semray.

Membrane thickness (µm)	Maximum DC (%)	Radiation time of maximum DC (s)	DC at 125 s radiation time (%)
200	62.3 ± 2.1	250	40.0 ± 3.3
150	44.6 ± 4.6	225	34.7 ± 2.7
100	40.2 ± 2.2	150	34.0 ± 2.5
50	37.2 ± 4.4	125	-

Next, the polymer mixture was cast on a PP/PE support to increase the mechanical strength of the resulting membrane and to enhance the practical feasibility during upscaling on a roll-to-roll system

to synthesize flat-sheet membranes. Using a support results in a lower DC (52.7 ± 8.7 % *vs* 62.3 ± 2.1 %) and requires a longer radiation time (250 s *vs* 300 s). This PP/PE support interferes in the propagation of UV light to the supporting metal plate. This statement is obviously only valid if there is interpenetration of the membrane into the support, which can be observed in the SEM images (Figure 9). Indeed, this non-woven support additionally absorbs and scatters the UV-light, decreasing the exposure of the metal plate to UV-irradiance. Less heat is thus build-up in the plate. In addition, the heat transfer to the acrylate layer is now less efficient due to the presence of the highly porous PP/PE support. Hence, the overall membrane temperature of the acrylate layer is much lower.

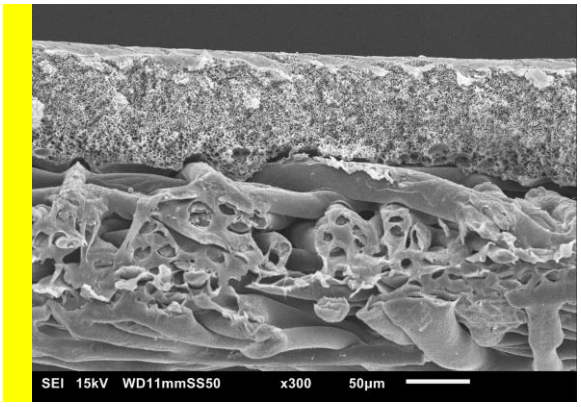

Figure 9. Cross-sectional SEM image for membrane composition M4 with support and UV radiated for 300 s.

3.7. Tensile strength

As a semi-interpenetrating network was formed during UV-LED curing, the tensile extension at maximum load decreased significantly. For an unsupported 200 µm thick polymer film prepared from 3.0 wt% TPO and 10.0 wt% SR 399LV, the non-cured membrane sample has an elongation of 9.3 mm for a maximum load of 7.9 N compared to a cured membrane sample (with a DC of 52.0 %) with an elongation of 0.8 mm for a maximum load of 9.0 N. As can be expected for a cross-linked polymer network, the cured membrane indeed became mechanically stronger as its maximum load increased at the cost of increased brittleness compared to a non-cured membrane [45].

In Table 5, the tensile strength values are given for different membrane types. For the same chemical composition but for a different membrane thickness (150 *vs* 200 µm), the tensile strength doubled for a non-cured membrane (3.9 *vs* 7.9 N). When both membranes were cured, they became stronger (larger maximum load) but more brittle when stretch forces were applied. Other chemical compositions with similar DC were also compared and showed a similar trend.

Table 5. DC (%), maximum loads (N) and tensile extension (mm) for different membrane coupons. UV-radiation was performed with UV-LED from Semray.

Membrane type	Thickness (µm)	DC (%)	Maximum load (N)	Tensile extension at max. load (mm)
M 5	200	52.0	9.0	0.8
	200	non-cured	7.9	9.3
M 5	150	49.0	4.4	0.7
	150	non-cured	3.9	3.2
M 2	200	55.0	9.2	1.9
	200	non-cured	8.2	5.4
M 3	200	49.0	8.9	1.5
	200	non-cured	7.3	8.5
M 10	200	29.0	8.2	0.8
	200	non-cured	7.3	2.7

3.8. Filtration performance

For filtration experiments, M 4 composition was used. Based on the results described in detail above, the photo-initiator TPO was selected for the membrane synthesis. An 'upscaled' sample of 6750 mm² was cured by the UV-LED of UVio Ltd. for 125 s. After curing, the membrane samples were stored in aluminum foil to preserve their moisture content or alternatively soaked for 48 h in a beaker with conditioning agents, i.e. a 40.0 % (v/v) glycerol solution in propan-2-ol (here referred to as Alu and IPA, respectively). After curing, a significant impact of the conditioning agent could be observed on the retention values (31.4 ± 5.2 % *vs* 50.7 ± 6.8 %, see Figure 10). The permeance, on the other hand, remained rather constant (0.22 ± 0.09 *vs* 0.33 ± 0.11 $L.m^{-2}.h^{-1}.bar^{-1}$). Thus, it is essential to store the membranes in a wet state as the lower retention observed for the dry membranes is most likely a consequence of the formation of small cracks, due to a combination of shrinkage by post-reticulation and drying of the sample. Next, when cured and non-cured samples were compared, both stored in conditioning agents, a significant decrease in permeance was observed upon curing (0.33 ± 0.11 *vs* 2.16 ± 0.45 $L.m^{-2}.h^{-1}.bar^{-1}$, respectively) while the retention was in the same order of magnitude (50.7 ± 6.8 % *vs* 61.0 ± 10.9 %). This can be explained by the densification of the membrane top layer during UV-curing. However, formation of defects caused by reticulation explained the absence of an increased retention. It is important to note here that the average retentions are not problematic as the as-prepared membranes are not meant to be used as such but as support for a more selective top-layer. Indeed, the main goal of this work was to prepare a more solvent-resistant membrane.

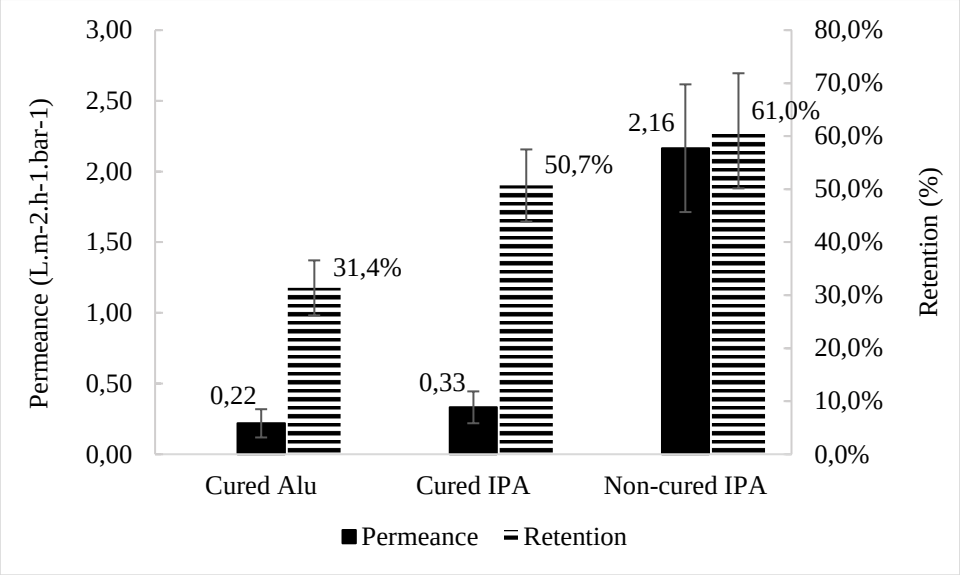

Figure 10. Influence of membrane storage conditions and UV-curing on performance of UV-cured PSU-membranes. UV-radiation was performed with UV-LED from Semray.

4. Conclusions

Investigating the impact of (non-)compositional parameters on the cross-linking efficiency showed that the cross-linker has a more important influence on the acrylate DC than the photo-initiator. The UV-LED system can be considered as a reproducible and feasible method for cross-linking this type of chemical composition. No significant difference in cross-linking efficiency could be observed between different UV-LED suppliers while a continuous radiation proved more efficient than a pulsed configuration. Additionally, a reduced film thickness was applied to reduce costs, but this resulted in a decreased DC. When implementing a non-woven support underneath the cast film, which would be essential during upscaling, a reduction in cross-linking degree of about 10.0% needs to be taken into account. As expected, the UV-curing resulted at the same time in a stronger polymer network, but also in a less flexible, structure of the membrane. Finally, the filtration performance of UV-cured PSU-membranes confirmed that the reported fabrication procedure is viable, yielding a more solvent tolerant PSU UF membrane [46].

Acknowledgements

The authors acknowledge sponsoring from the research foundation of Flanders (FWO) in the frame of a post-doctoral grant (12Y3919N-ND). The authors are further grateful for the financial support from the C16/17/005 funding from KU Leuven, the Flemish/Dutch Government through an SBO-STW grant (Nanomexico). We are also grateful for the support of Polytec GmbH and UVio Ltd by providing us with the UV-LED test set-up and information.

5. Data availability

The raw/ processed data required to reproduce these findings cannot be shared at this time as the data also forms part of an ongoing study.

References

[1] esteana, Waste, Horizon 2020 - European Commission. (2014). https://ec.europa.eu/programmes/horizon2020/en/h2020-section/waste (accessed March 13, 2019).

[2] N.N. Li, A.G. Fane, W.S.W. Ho, T. Matsuura, Advanced Membrane Technology and Applications, John Wiley & Sons, 2011.

[3] H. Strathmann, L. Giorno, E. Drioli, An Introduction to Membrane Science and Technology, (n.d.) 29.

[4] Vision 2020: 2000 Separations Roadmap, United States. Department of Energy. Office of Energy Efficiency and Renewable Energy, 2000.

[5] J. Mulder, Basic Principles of Membrane Technology, Springer Science & Business Media, 2012.

[6] N.L. Le, S.P. Nunes, Materials and membrane technologies for water and energy sustainability, Sustainable Materials and Technologies. 7 (2016) 1–28. doi:10.1016/j.susmat.2016.02.001.

[7] A.K. Hołda, I.F.J. Vankelecom, Understanding and guiding the phase inversion process for synthesis of solvent resistant nanofiltration membranes, Journal of Applied Polymer Science. 132 (n.d.). doi:10.1002/app.42130.

[8] P. Marchetti, M.F.J. Solomon, G. Szekely, A.G. Livingston, Molecular Separation with Organic Solvent Nanofiltration: A Critical Review, (2014). doi:10.1021/cr500006j.

[9] S. Hermans, E. Dom, H. Mariën, G. Koeckelberghs, I.F.J. Vankelecom, Efficient synthesis of interfacially polymerized membranes for solvent resistant nanofiltration, Journal of Membrane Science. 476 (2015) 356–363. doi:10.1016/j.memsci.2014.11.046.

[10] P. Vandezande, L.E. M. Gevers, I.F. J. Vankelecom, Solvent resistant nanofiltration: separating on a molecular level, Chemical Society Reviews. 37 (2008) 365–405. doi:10.1039/B610848M.

[11] M. Mertens, C. Van Goethem, M. Thijs, G. Koeckelberghs, I.F.J. Vankelecom, Crosslinked PVDF-membranes for solvent resistant nanofiltration, Journal of Membrane Science. 566 (2018) 223–230. doi:10.1016/j.memsci.2018.08.051.

[12] C. Van Goethem, M. Mertens, I.F.J. Vankelecom, Crosslinked PVDF membranes for aqueous and extreme pH nanofiltration, Journal of Membrane Science. 572 (2019) 489–495. doi:10.1016/j.memsci.2018.11.036.

[13] S. Hermans, H. Mariën, C. Van Goethem, I.F. Vankelecom, Recent developments in thin film (nano)composite membranes for solvent resistant nanofiltration, Current Opinion in Chemical Engineering. 8 (2015) 45–54. doi:10.1016/j.coche.2015.01.009.

[14] K. Vanherck, P. Vandezande, S.O. Aldea, I.F.J. Vankelecom, Cross-linked polyimide membranes for solvent resistant nanofiltration in aprotic solvents, Journal of Membrane Science. 320 (2008) 468–476. doi:10.1016/j.memsci.2008.04.026.

[15] N. Daems, S. Milis, R. Verbeke, A. Szymczyk, P.P. Pescarmona, I.F.J. Vankelecom, High-performance membranes with full pH-stability, RSC Adv. 8 (2018) 8813–8827. doi:10.1039/C7RA13663C.

[16] Z. Beril Gönder, S. Arayici, H. Barlas, Advanced treatment of pulp and paper mill wastewater by nanofiltration process: Effects of operating conditions on membrane fouling, Separation and Purification Technology. 76 (2011) 292–302. doi:10.1016/j.seppur.2010.10.018.

[17] Acid mine drainage treatment by nanofiltration_ A study of membrane fouling, chemical cleaning, and membrane ageing | Elsevier Enhanced Reader, (n.d.). doi:10.1016/j.seppur.2017.09.043.

[18] Integration of nanofiltration and reverse osmosis for metal separation and sulfuric acid recovery from gold mining effluent | Elsevier Enhanced Reader, (n.d.). doi:10.1016/j.seppur.2015.08.040.

[19] D. Fritsch, P. Merten, K. Heinrich, M. Lazar, M. Priske, High performance organic solvent nanofiltration membranes: Development and thorough testing of thin film composite membranes made of polymers of intrinsic microporosity (PIMs), Journal of Membrane Science. 401–402 (2012) 222–231. doi:10.1016/j.memsci.2012.02.008.

[20] I.B. Valtcheva, S.C. Kumbharkar, J.F. Kim, L.G. Peeva, A.G. Livingston, Development of Organic Solvent Nanofiltration Membranes for the Application in Extreme pH Conditions, Procedia Engineering. 44 (2012) 313–315. doi:10.1016/j.proeng.2012.08.399.

[21] L. Pérez-Manríquez, J. Aburabi'e, P. Neelakanda, K.-V. Peinemann, Cross-linked PAN-based thin-film composite membranes for non-aqueous nanofiltration, Reactive and Functional Polymers. 86 (2015) 243–247. doi:10.1016/j.reactfunctpolym.2014.09.015.

[22] M.F. Jimenez Solomon, Y. Bhole, A.G. Livingston, High flux hydrophobic membranes for organic solvent nanofiltration (OSN)—Interfacial polymerization, surface modification and solvent activation, Journal of Membrane Science. 434 (2013) 193–203. doi:10.1016/j.memsci.2013.01.055.

[23] K. Majewska-Nowak, Synthesis and properties of polysulfone membranes, Desalination. 71 (1989) 83–95. doi:10.1016/0011-9164(89)80001-3.

[24] I. Strużyńska-Piron, J. Loccufier, L. Vanmaele, I.F.J. Vankelecom, Parameter Study on the Preparation of UV Depth-Cured Chemically Resistant Polysulfone-Based Membranes, Macromolecular Chemistry and Physics. 215 (2014) 614–623. doi:10.1002/macp.201300713.

[25] V.R. Sastri, High-Temperature Engineering Thermoplastics, in: Plastics in Medical Devices, Elsevier, 2010: pp. 175–215. doi:10.1016/B978-0-8155-2027-6.10008-X.

[26] L.W. McKeen, High Temperature/High Performance Polymers, in: Film Properties of Plastics and Elastomers, Elsevier, 2012: pp. 315–337. doi:10.1016/B978-1-4557-2551-9.00012-8.

[27] D.V. Rosato, D.V. Rosato, Plastics, in: Reinforced Plastics Handbook, Elsevier, 2005: pp. 109–211. doi:10.1016/B978-185617450-3/50005-0.

[28] A.K. Hołda, I.F.J. Vankelecom, Integrally skinned PSf-based SRNF-membranes prepared via phase inversion—Part A: Influence of high molecular weight additives, Journal of Membrane Science. 450 (2014) 512–521. doi:10.1016/j.memsci.2013.08.050.

[29] K. Vanherck, G. Koeckelberghs, I.F.J. Vankelecom, Crosslinking polyimides for membrane applications: A review, Progress in Polymer Science. 38 (2013) 874–896. doi:10.1016/j.progpolymsci.2012.11.001.

[30] A.K. Hołda, B. Aernouts, W. Saeys, I.F.J. Vankelecom, Study of polymer concentration and evaporation time as phase inversion parameters for polysulfone-based SRNF membranes, Journal of Membrane Science. 442 (2013) 196–205. doi:10.1016/j.memsci.2013.04.017.

[31] X. Chen, A Thermally Re-mendable Cross-Linked Polymeric Material, Science. 295 (2002) 1698–1702. doi:10.1126/science.1065879.

[32] M.E. Rezac, E. Todd Sorensen, H.W. Beckham, Transport properties of crosslinkable polyimide blends, Journal of Membrane Science. 136 (1997) 249–259. doi:10.1016/S0376-7388(97)00170-1.

[33] A.M. Kratochvil, W.J. Koros, Decarboxylation-Induced Cross-Linking of a Polyimide for Enhanced CO_2 Plasticization Resistance, Macromolecules. 41 (2008) 7920–7927. doi:10.1021/ma801586f.

[34] X. Li, P. Vandezande, I.F.J. Vankelecom, Polypyrrole modified solvent resistant nanofiltration membranes, Journal of Membrane Science. 320 (2008) 143–150. doi:10.1016/j.memsci.2008.03.061.

[35] G. Kang, Y. Cao, Application and modification of poly(vinylidene fluoride) (PVDF) membranes – A review, Journal of Membrane Science. 463 (2014) 145–165. doi:10.1016/j.memsci.2014.03.055.

[36] Q. Bi, Q. Li, Y. Tian, Y. Lin, X. Wang, Hydrophilic modification of poly(vinylidene fluoride) membrane with poly(vinyl pyrrolidone) via a cross-linking reaction, Journal of Applied Polymer Science. 127 (n.d.) 394–401. doi:10.1002/app.37629.

[37] A. Taguet, B. Ameduri, B. Boutevin, Crosslinking of Vinylidene Fluoride-Containing Fluoropolymers, in: Crosslinking in Materials Science, Springer, Berlin, Heidelberg, 2005: pp. 127–211. doi:10.1007/b136245.

[38] A.A. Yushkin, M.N. Efimov, A.A. Vasilev, Y.G. Bogdanova, V.D. Dolzhikova, G.P. Karpacheva, A.V. Volkov, Modification of polyacrylonitrile membranes by incoherent IR radiation, Pet. Chem. 57 (2017) 341–346. doi:10.1134/S0965544117040089.

[39] A.A. Yushkin, M.N. Efimov, A.A. Vasil'ev, V.I. Ivanov, Y.G. Bogdanova, V.D. Dolzhikova, G.P. Karpacheva, G.N. Bondarenko, A.V. Volkov, Effect of IR Radiation on the Properties of Polyacrylonitrile and Membranes on Its Basis, Polym. Sci. Ser. A. 59 (2017) 880–890. doi:10.1134/S0965545X17060104.

[40] Y. Liu, C. Pan, M. Ding, J. Xu, Effect of crosslinking distribution on gas permeability and permselectivity of crosslinked polyimides, European Polymer Journal. 35 (1999) 1739–1741. doi:10.1016/S0014-3057(98)00255-9.

[41] V. Altun, J.-C. Remigy, I.F.J. Vankelecom, UV-cured polysulfone-based membranes: Effect of co-solvent addition and evaporation process on membrane morphology and SRNF performance, Journal of Membrane Science. 524 (2017) 729–737. doi:10.1016/j.memsci.2016.11.060.

[42] S. Behnke, M. Ulbricht, Thin-film composite membranes for organophilic nanofiltration based on photo-cross-linkable polyimide, Reactive and Functional Polymers. 86 (2015) 233–242. doi:10.1016/j.reactfunctpolym.2014.09.027.

[43] D. He, H. Susanto, M. Ulbricht, Photo-irradiation for preparation, modification and stimulation of polymeric membranes, Progress in Polymer Science. 34 (2009) 62–98. doi:10.1016/j.progpolymsci.2008.08.004.

[44] V. Altun, M. Bielmann, I.F.J. Vankelecom, Study of phase inversion parameters for EB-cured polysulfone-based membranes, RSC Advances. 6 (2016) 110916–110921. doi:10.1039/C6RA24340A.

[45] E. Andrzejewska, Free Radical Photopolymerization of Multifunctional Monomers, in: Three-Dimensional Microfabrication Using Two-Photon Polymerization, Elsevier, 2016: pp. 62–81. doi:10.1016/B978-0-323-35321-2.00004-2.

[46] P.-R. Van den Mooter, N. Daems, I.F.J. Vankelecom, Preparation of solvent resistant supports through formation of a semi-interpenetrating polysulfone/polyacrylate network using UV cross-linking – Part 1: Selection of optimal UV curing conditions, Reactive and Functional Polymers. 136 (2019) 189–197. doi:10.1016/j.reactfunctpolym.2018.12.015.

[47] J.S. Kang, J. Won, H.C. Park, U.Y. Kim, Y.S. Kang, Y.M. Lee, Morphology control of asymmetric membranes by UV irradiation on polyimide dope solution, Journal of Membrane Science. 169 (2000) 229–235. doi:10.1016/S0376-7388(99)00340-3.

[48] J. Park, T.-H. Kim, H.J. Kim, J.-H. Choi, Y.T. Hong, Crosslinked sulfonated poly(arylene ether sulfone) membranes for fuel cell application, International Journal of Hydrogen Energy. 37 (2012) 2603–2613. doi:10.1016/j.ijhydene.2011.10.122.

[49] Preparation of solvent resistant supports through formation of a semi-interpenetrating polysulfone/polyacrylate network using UV cross-linking – Part 1_ Selection of optimal UV curing conditions | Elsevier Enhanced Reader, (n.d.). doi:10.1016/j.reactfunctpolym.2018.12.015.

[50] Semray ® UV LED Plug & Play System, (n.d.). https://www.heraeus.com/en/hng/products_and_solutions/uv_lamps_and_systems/semray_uv_led_systems.aspx (accessed March 26, 2019).

[51] (n.d.). http://www.excelitas.com/Pages/Product/OmniCure-AC-8-Series.aspx (accessed June 25, 2018).

[52] Cary 620 FTIR Microscopes | Agilent, (n.d.). https://www.agilent.com/en/products/ftir/ftir-microscopes-imaging-systems/cary-620-ftir-microscopes (accessed June 25, 2018).

[53] Williams, Spectroscopic Meth. In Organic Chemistry, McGraw-Hill Education (India) Pvt Limited, n.d.

[54] Membrane Technology Group | Pilot – cMACS, (n.d.). https://www.biw.kuleuven.be/m2s/cmacs/research/membrane-technology/Pilot (accessed July 15, 2019).

[55] M. Hancock, E. Hawes, F. Yang, E. Grulke, Crosslinking gradients of a photopolymerized multifunctional acrylate film control mechanical properties, J Coat Technol Res. 16 (2019) 1153–1163. doi:10.1007/s11998-019-00191-9.

[56] C.E. Hoyle, J.F. Kinstle, Radiation Curing of Polymeric Materials, Radiation Curing of Polymeric Materials / Volume 417 of ACS Symposium Series, Eds. Charles E Hoyle and James F Kinstle. Washington DC : American Chemical Society, C1990. 417 (1990). doi:10.1021/bk-1990-0417.

[57] N. KRISHNAMURTHY, P. VALLINAYAGAM, D. MADHAVAN, ENGINEERING CHEMISTRY, PHI Learning, 2014.

[58] L. Macarie, G. Ilia, The influence of temperature and photoinitiator concentration on photoinitiated polymerization of diacrylate monomer, Open Chemistry. 3 (2005). doi:10.2478/BF02475199.

[59] R.C. Alonso, W. Brandt, E.J. Souza-Junior, R. Puppin-Rontani, M.A. Sinhoreti, Photoinitiator concentration and modulated photoactivation: influence on polymerization characteristics of experimental composites, Appl Adhes Sci. 2 (2014) 10. doi:10.1186/2196-4351-2-10.

[60] S. Ahmad, J. Stejny, Polymerisation, structure and track recording properties of CR-39, International Journal of Radiation Applications and Instrumentation. Part D. Nuclear Tracks and Radiation Measurements. 19 (1991) 11–16. doi:10.1016/1359-0189(91)90135-5.

[61] S. Keskin, S. Jockusch, N.J. Turro, N. Arsu, 2-Mercaptothioxanthone as Sensitizer and Coinitiator for Acylphosphine Oxide Photoinitiators for Free Radical Polymerization, Macromolecules. 41 (2008) 4631–4634. doi:10.1021/ma800472u.

[62] J.E. Baxter, R. Stephen Davidson, H.J. Hageman, Acylphosphine oxides as photoinitiators for acrylate and unsaturated polyester resins, European Polymer Journal. 24 (1988) 419–424. doi:10.1016/0014-3057(88)90077-8.

[63] L.R. Gatechair, D. Wostratzky, Photoinitiators: A Review of Mechanisims and Applications, in: L.-H. Lee (Ed.), Adhesive Chemistry, Springer US, Boston, MA, 1984: pp. 409–438. doi:10.1007/978-1-4613-2435-5_22.

[64] W. Schrof, E. Beck, R. Königer, W. Reich, R. Schwalm, Depth profiling of UV cured coatings containing photostabilizers by confocal Raman microscopy, Progress in Organic Coatings. 35 (1999) 197–204. doi:10.1016/S0300-9440(99)00026-0.

List of Figures

List of Tables